
A COMPUTATIONALLY EFFICIENT NEURAL NETWORK FOR PREDICTING WEATHER FORECAST PROBABILITIES

THIS MANUSCRIPT IS A NON-PEER REVIEWED PREPRINT THAT HAS BEEN SUBMITTED FOR REVIEW IN
QUARTERLY JOURNAL OF THE ROYAL METEOROLOGICAL SOCIETY.

Mariana C A Clare
Imperial College London,
London, UK
m.clare17@imperial.ac.uk

Omar Jamil
University of Exeter,
Exeter, UK
(formerly Met Office, Exeter, UK)

Cyril Morcrette
Met Office,
Exeter, UK

May 30, 2022

ABSTRACT

The success of deep learning techniques over the last decades has opened up a new avenue of research for weather forecasting. Here, we take the novel approach of using a neural network to predict probability density functions rather than a single output value, thus producing a probabilistic weather forecast. This enables the calculation of both uncertainty and skill metrics for the neural network predictions, and overcomes the common difficulty of inferring uncertainty from these predictions.

This approach is purely data-driven and the neural network is trained on the WeatherBench dataset (processed ERA5 data) to forecast geopotential and temperature 3 and 5 days ahead. An extensive data exploration leads to the identification of the most important input variables, which are also found to agree with physical reasoning, thereby validating our approach. In order to increase computational efficiency further, each neural network is trained on a small subset of these variables. The outputs are then combined through a stacked neural network, the first time such a technique has been applied to weather data. Our approach is found to be more accurate than some numerical weather prediction models and as accurate as more complex alternative neural networks, with the added benefit of providing key probabilistic information necessary for making informed weather forecasts.

Keywords Deep learning, Probabilistic weather forecasting, Probability density functions, ResNet, Stacked neural network, Ensemble dropout, Data exploration

1 Introduction

For over 100 years, advanced mathematical techniques have been used for weather prediction. Today, Numerical Weather Prediction (NWP) is an advanced discipline which uses some of the world's largest supercomputers to solve complex non-linear differential equations. The forecast skill of these models has been improving by approximately one day every ten years, *i.e.*, the 5-day forecast today is as accurate as the 4-day forecast was ten years ago (see Bauer et al., 2015). This improvement has been achieved through the scientific and technological development of both NWP models and computers (Bauer et al., 2015). However, the success of deep learning techniques over the last decade has opened up a new avenue for weather forecasting (Schultz et al., 2021). Research has been mainly focused on the supervised learning techniques of neural networks (Dueben and Bauer, 2018; Brenowitz and Bretherton, 2019; Rasp et al., 2020;

Rasp and Thuerey, 2020; Weyn et al., 2020) and random forests (Yuval and O’Gorman, 2020). Some works, such as Brenowitz and Bretherton (2019), have successfully coupled neural networks with General Circulation Models to emulate physical parametrisations, whilst others have taken a purely data driven approach (Rasp and Thuerey, 2020). In this work, we take the data-driven approach and use residual neural networks to create 3-day and 5-day hindcasts.

A limitation of the deep learning approaches used in the works referred to above is that it is difficult to infer the uncertainty of the predictions from their results (Schultz et al., 2021). Whereas previous works address these limitations by making use of model ensembles (Bihlo, 2021) or training on hindcast error and ensemble spread (Scher and Messori, 2018), here we take the novel approach of using neural network architectures that predict probability density functions for the output variable instead of single values. These density functions allow practitioners to estimate the uncertainty of the neural network outputs and make a more informed weather forecast. In order to optimise memory use and model accuracy, we train multiple neural networks on a small number of variables and combine their outputs using techniques such as a stacked neural network. This is a technique that has not been used with weather data before. In this work, the neural networks are trained on the WeatherBench dataset created by Rasp et al. (2020) and used to predict both a 3-day and a 5-day weather hindcast of geopotential at the 500hPa pressure level in m^2s^{-2} (hereafter Z500) and temperature at the 850hPa pressure level in Kelvin (K) (hereafter T850). These variables are chosen so that our results can be compared to those in other works which use the same dataset (Rasp et al., 2020; Rasp and Thuerey, 2020; Weyn et al., 2020).

The remainder of this work is structured as follows: Section 2 describes the data used in this study followed by the data exploration techniques and neural network models used; Section 3 presents results from using stacked neural networks to forecast weather data and shows how the output can be used to infer uncertainty; and finally Section 4 concludes the work.

2 Methods

2.1 Data

The WeatherBench dataset contains a mix of multi-levelled (13 pressure levels) and single level variables. These variables have been derived from the ERA5 dataset that has been regrided to a lower resolution. One of the benefits of deep learning is that we do not need to carry out extensive feature engineering and the neural networks are able to find the best predictors in the data. However, even with a lower resolution grid, this dataset is still too large to use in its entirety. We therefore first use data exploration techniques to determine which input variables are most relevant for prediction, and then train multiple neural networks on subsets of these variables.

2.2 Data Exploration and Feature Selection

A key component in the application of neural networks, or indeed any deep learning algorithm, is choosing appropriate data on which to train the model. This problem is two-fold: i) how many input variables and ii) how many individual data points to include. There is always a trade-off between having a large amount of data resulting in large computational and memory costs, and having too little data resulting in underfitting. The WeatherBench dataset produced by Rasp et al. (2020) contains a variety of weather variables and uses as its raw data the ERA5 reanalysis dataset (Hersbach et al., 2020) for the 40-year period from 1979 to 2018. The data was processed and regrided onto a 5.625° resolution latitude-longitude grid (32×64 grid points) by Rasp et al. (2020) and we refer the reader to this work for more details. Following the same work, we consider data from 1979 to 2016 to be the training dataset, with data from 2015 to 2016 used for validation, and consider 2017 to 2018 to be the test dataset.

Using every data variable to train the neural network would be computationally expensive and potentially unnecessary. We are also keen to explore a largely data-driven approach in this work so we look at different methods to find best predictors for the forecasts.

2.2.1 Correlation

A simple approach to determine which are the most important variables to include in the training dataset of the neural network is to calculate the Pearson correlation coefficient between the variables. In this work, due to memory constraints, our training datasets are only ever made up of Z500, T850 and at most one other variable type at the current time, t , (see Section 3). Thus, the correlations between other variables whilst interesting are not relevant to this work. In this section, we thus consider the correlations between all possible input variables at the current time t and Z500 and T850 in 3 days time, because these are the actual values we are trying to predict. The results are shown in Table I. We have also calculated the correlation with Z500 and T850 in 5 days time but have not shown the results

Variable names	Correlation Z500 (3 days)	Correlation T850 (3 days)
geopotential (max - 500hPa (Z500) 300hPa (T850))	0.999999	0.950847
temperature (max - 600hPa (Z500) 850hPa (T850))	0.955410	0.999999
2m temperature	0.881828	0.946909
hourly precipitation	0.079967	0.115602
relative humidity (max - 100hPa (Z500) 100hPa (T850))	0.447344	0.447228
specific humidity (max - 1000hPa (Z500) 1000hPa (T850))	0.814368	0.832719
total cloud cover	-0.252565	-0.240670
top-of-atmosphere incoming solar radiation	0.260928	0.278964
potential vorticity (max - 50hPa (Z500) 700hPa (T850))	0.252337	0.247780
relative vorticity (max - 50hPa (Z500) 50hPa (T850))	0.186012	0.142445
10m wind (x-direction)	-0.184053	-0.135853
10m wind (y-direction)	-0.032521	-0.050571
wind (x-direction) (max - 50hPa (Z500) 50hPa (T850))	-0.504442	-0.447946
wind (y-direction) (max - 850hPa (Z500) 850hPa (T850))	-0.029064	-0.042132
Constant - orography	-0.325298	-0.385886
Constant - land sea mask	-0.189865	-0.214283
Constant - latitude	0.236026	0.167379
Constant - longitude	0.006956	-0.001363
Constant - soil type	0.047839	0.040490

Table I: Correlation between Z500 and T850 in 3 days time and other variable types in the dataset.

here because there is almost no difference. (Note that as the constants are constant in time, this temporal distinction is meaningless for these variables).

For a Pearson correlation coefficient, a value close to 1 indicates a strong positive correlation, close to -1 indicates a strong negative correlation, and close to 0 indicates no correlation. However, there is no clear distinction as to when a correlation goes from being strong to being weak. When Konecny and Pustka (2017) and Yassaghi et al. (2019) consider correlation between weather data variables, they assume that an absolute value above 0.2 is indicative of an important relationship between the two variables. This value is low, but, given that our correlation analysis is simply an initial phase to exclude variables which are really not important, we make the same assumption. Thus, in Table I we have marked in red any correlations with an absolute value lower than 0.2. For ease of interpretation we have also marked in green any correlations with an absolute value above 0.5, as this has been considered a strong correlation in other fields (e.g. Buda, 2011). Where the variables have data on multiple pressure levels, we have calculated the correlation at all pressure levels but for simplicity include in the tables only the maximum correlation over all pressure levels. We determine optimum level choice later in Section 2.2.2.

Table I reveals that both components of the horizontal wind at the 10m level, the meridional (y-direction) wind at all pressure levels and surface precipitation are not correlated with Z500 and T850, and can therefore be excluded from our training dataset. We keep top-of-atmosphere solar radiation as it is the energy source driving the system. The table also shows a higher correlation with potential vorticity than with relative vorticity. Thus, taking a pragmatic approach, we discard relative vorticity from our dataset, and assume that one vorticity variable will be sufficient. For humidity, the table shows that specific humidity is more strongly correlated with Z500 and T850 than relative humidity. Again, we assume that a single humidity variable is sufficient and discard relative humidity.

Finally, the correlations between Z500 and T850 and the constant fields show, that there is almost no correlation between them and soil type so we discard that variable. Unsurprisingly, there is also essentially no correlation with longitude, so that is discarded too, but we keep the latitude and land sea mask as these variables have correlation values with a magnitude above 0.2 for either Z500 or T850.

Thus, as a result of the analysis in this section, we have been able to exclude 45 variables from the training dataset out of a total of 115 (where for data on multiple levels, we are counting each individual level as a variable). For the remaining variables, we require further analysis.

2.2.2 Variable and level importance

After the correlation analysis, the set of relevant input variables is formed by the multi-level fields of geopotential, temperature, specific humidity, potential vorticity and zonal wind (x -direction) and the single-level fields of 2m tem-

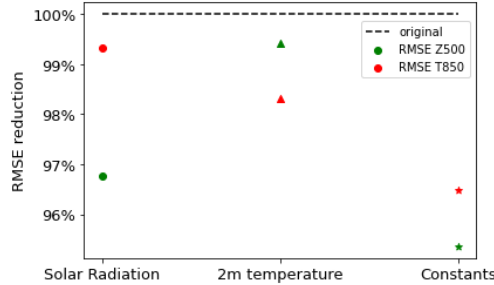


Figure 1: Percentage error reduction at inference from training using extra single-level variables. These are: just incoming top-of-atmosphere solar radiation, just 2m temperature, or the three constants of orography, land-sea mask and latitude. Results are calculated from the mean of 32 ensemble members generated using dropout at inference.

perature, top-of-atmosphere incoming solar radiation and constants (the three variables constant in time – orography, land sea mask, and latitude). This gives a total of 70 single-level variables.

In order to further refine the set of relevant variables, we first train an individual neural network with an input dataset of just Z500 and T850, and define this as our ‘original’ training dataset, which will be used as a benchmark to understand the effect of including other variables on the final error. The architecture of this network is a convolutional ResNet (see Section 2.3) with 5 residual blocks and dropout. We use the dropout at inference technique to extract an ensemble of 32 outputs from the single trained model, and then calculate the error of the ensemble mean (see Section 2.3.2). By using this, we average out some of the randomness of the results. We then train individual neural networks with an input dataset of Z500 and T850 and one variable from the relevant list, and compare it to the original benchmark. Note that throughout this section, we have chosen to focus on improving the 3-day hindcast and assume that any improvements in methodology for this will also result in improvements in the 5-day hindcast. Thus unless explicitly stated all results shown are for the 3-day hindcast.

We start by considering the significance of the variables which are only defined at a single height: 2m temperature, total incident solar radiation and constants. The resultant ensemble errors are shown in Figure 1 as a percentage of the error from the benchmark dataset. The figure shows that solar radiation is relatively unimportant for predicting T850 and relatively important for predicting Z500, that 2m temperature is relatively unimportant for predicting Z500 and T850 and finally constants are important for predicting both Z500 and T850. Thus from Figure 1, we conclude that we can exclude 2m temperature from both training datasets and solar radiation from the T850 training dataset.

Finally, we seek to understand which pressure levels are the most important in predicting Z500 and T850. We do this using a purely data-driven approach, but in Section 2.2.3 note that the results from a data-driven approach often agree with well-established theory in meteorology. For all multi-level input variables (geopotential, temperature, specific humidity, potential vorticity and zonal wind), we consider multiple different level combinations again using a 5 block convolutional ResNet with dropout. As before, we use the dropout at inference technique to extract an ensemble of 32 outputs from the single trained model, and then calculate the error of the ensemble mean.

To determine the optimum levels for the geopotential and temperature variables, we proceed in a systematic way. First we consider the two levels we are trying to predict and the levels between these two; (*i.e.* [500hPa, 600hPa, 700hPa, 850hPa]); next we extend this dataset by including the two higher pressure levels (*i.e.* [500hPa, 600hPa, 700hPa, 850hPa, 925hPa, 1000hPa]); then we add the two lower pressure levels to the first dataset (*i.e.* [300hPa, 400hPa, 500hPa, 600hPa, 700hPa, 850hPa]); then we include both the two lower and two higher pressure levels (*i.e.* [300hPa, 400hPa, 500hPa, 600hPa, 700hPa, 850hPa, 950hPa and 1000hPa]), and finally we add two further low pressure levels (*i.e.* [100hPa, 250hPa, 300hPa, 400hPa, 500hPa, 600hPa, 700hPa, 850hPa, 950hPa and 1000hPa]). The results of this analysis for the geopotential variable are shown in Figures 2a and 2b. For the temperature variable they are shown in Figures 2c and 2d. They show that for both Z500 and T850, in general, including more pressure levels results in a larger reduction in error, but this must be balanced with computational cost. When predicting Z500, a good compromise for both the geopotential and temperature input variables is the level choice [300, 400, 500, 600, 700, 850] (the green stars on Figures 2a and 2b). On the other hand, when predicting T850, a good compromise for both the geopotential and temperature input variables is the level choice [500hPa, 600hPa, 700hPa, 850hPa, 925hPa, 1000hPa] (the orange stars on Figures 2c and 2d). Given that T850 is a higher pressure level than Z500, it is unsurprising that the T850 level choice contains higher pressure levels than the Z500 level choice.

For the other variables, the same analysis does not apply. When conducting the correlation analysis in Section 2.2.1, we determined that the correlation for specific humidity is greatest at the higher pressure levels (see Table I). Thus, we

begin by considering the higher pressure levels (*i.e.* [600hPa, 700hPa, 850hPa, 925hPa, 1000hPa]), then add different subsets of the lower pressure levels, and finally consider a broad range of pressure levels (*i.e.* [150hPa, 200hPa, 250hPa, 300hPa, 500hPa, 600hPa, 700hPa, 850hPa, 925hPa, 1000hPa]). Figures 2e and 2f show the results of this analysis and that, unlike with the temperature and geopotential input variables, adding more pressure levels does not always result in a reduction in error. This may be because when more levels are added, information from unimportant levels dominates the predictions leading to errors. An appropriate level choice for specific humidity is thus [150hPa, 200hPa, 600hPa, 700hPa, 850hPa, 925hPa, 1000hPa] (the orange stars on Figures 2e and 2f) for both Z500 and T850 prediction.

For potential vorticity, the correlation analysis in Table I shows that the most important levels are at either end of the pressure level spectrum. Thus when determining the right level choice, we consider groupings of levels at both high and low pressures. We also consider the middle pressure levels shifted to the higher end of the pressure spectrum (*i.e.* [250hPa, 300hPa, 400hPa, 500hPa, 700hPa, 850hPa, 925hPa, 1000hPa]) and to the lower end of the pressure spectrum (*i.e.* [50hPa, 100hPa, 150hPa, 250hPa, 300hPa, 400hPa, 500hPa, 850hPa, 925hPa]). Figures 2g and 2h show that there does not seem to be a clear pattern between level choice and error reduction for potential vorticity. However, the level choice of [150hPa, 250hPa, 300hPa, 700hPa, 850hPa] (the green stars on Figures 2g and 2h) results in a large error reduction in both RMSE Z500 and RMSE T850 and is also cheap in memory cost and so is an appropriate level choice for potential vorticity.

Finally we consider the zonal wind input variable. Using the correlation analysis, the most important levels are at either end of the pressure spectrum. Thus we consider groupings of levels at both low and high pressures. We also consider larger groupings at the higher end of the pressure spectrum (*i.e.* [300hPa, 400hPa, 500hPa, 600hPa, 700hPa, 850hPa, 925hPa, 1000hPa]) to check if the lower pressures are affecting the results. Figures 2i and 2j show that for both Z500 and T850 having levels at both low and high pressures is important for reducing error. In both cases, we choose the level grouping of [50hPa, 100hPa, 300hPa, 850hPa, 925hPa, 1000hPa] (the orange stars on Figures 2i and 2j) as an appropriate choice because it results in a large error reduction and is also cheap in memory cost. This concludes our data-driven level importance section.

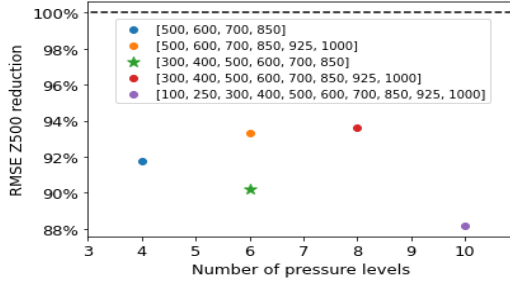
2.2.3 Agreement with meteorological theory

So far, a purely data-driven approach has been adopted. Variables have been assessed in terms of the benefit they bring, with little meteorological consideration for what a physically sensible set should be. Having found the most useful input variables, it is now sensible to look back and comment. It is worth emphasizing that the focus has been on predicting Z500 and T850 three days ahead. If other input variables, or other lead-times, had been the focus of the predictions, then other inputs may have been found to be beneficial.

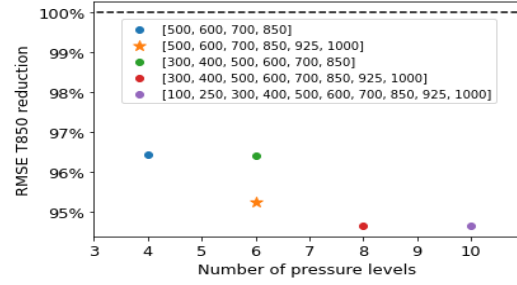
Through the correlation analysis, we exclude relative humidity from our training dataset because it has a lower correlation with the variables of interest than specific humidity. From a physical perspective, we would expect little gain from using relative humidity as this variable is a function of specific humidity, temperature and pressure (which is itself related to geopotential), which are all already included in the training dataset. Similarly, we exclude relative vorticity and keep potential vorticity because of the latter's higher correlation. The relative vorticity describes the rotational component of the horizontal flow. However potential vorticity also includes a contribution from the vertical stratification of the temperature field and is known to be a conserved variable in adiabatic flow. It is often used in the study of the development of mid-latitude weather systems and as a result, it is not surprising that its inclusion is more beneficial in these predictions.

In addition, through our analysis, we have identified the pressure levels that have the most impact in determining Z500 and T850. These choices are all supported by physical reasoning:

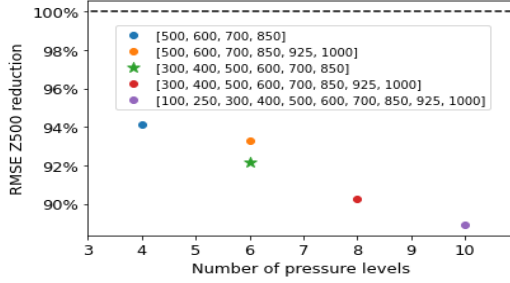
- Geopotential & Temperature: Using physical intuition, we would expect that the levels that are most important for prediction are those above and below the level of interest (e.g. Hoskins et al., 1978). In addition temperature and geopotential are linked through the hypsometric equation which relates the thickness of the geopotential to the temperature (e.g. Wallace and Hobbs, 1977). Thus it is physically consistent that the most important levels of geopotential to predict Z500 are the same as those for temperature (and the same is true for T850).
- Specific humidity: This variable is greatest in magnitude near the surface (Wang and Wang, 2014) and thus the levels near the surface being important agrees with physical reasoning.
- Potential vorticity: By including the levels near the tropopause (e.g. 150 hPa) and just above the boundary-layer (e.g. 850 hPa) in our training dataset, we are allowing the neural network to learn about the interactions between lower and upper level potential vorticity which can accelerate cyclone development (e.g. Hoskins, 2015).



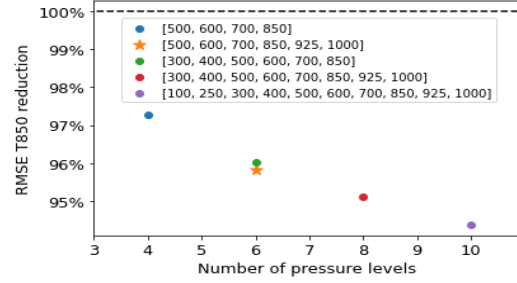
(a) Geopotential: Error reduction for Z500.



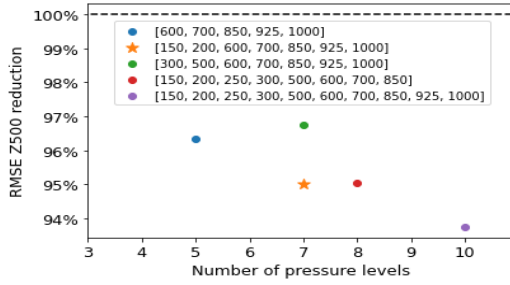
(b) Geopotential: Error reduction for T850.



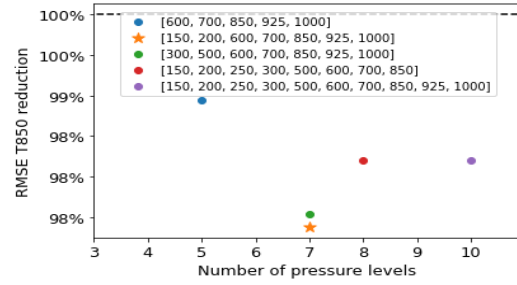
(c) Temperature: Error reduction for Z500.



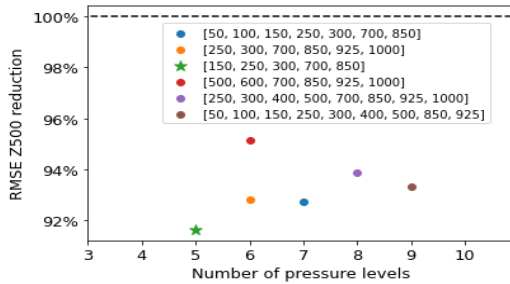
(d) Temperature: Error reduction for T850.



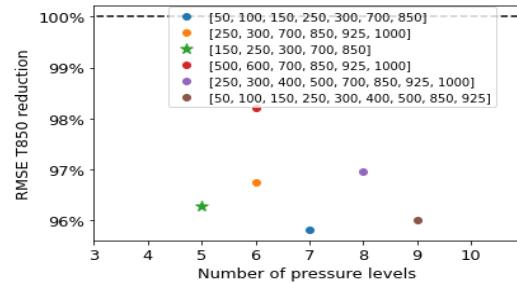
(e) Specific humidity: Error reduction for Z500.



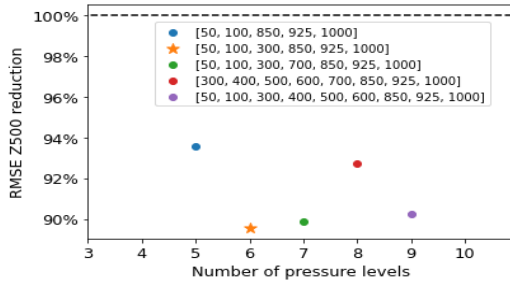
(f) Specific humidity: Error reduction for T850.



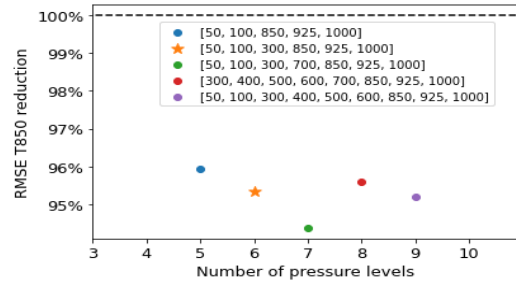
(g) Potential vorticity: Error reduction for Z500.



(h) Potential vorticity: Error reduction for T850.



(i) Zonal wind: Error reduction for Z500.



(j) Zonal wind: Error reduction for T850.

Figure 2: Percentage error reduction at inference from training using extra variable levels (chosen levels are marked with a star). Results are the mean of 32 ensemble members generated using dropout at inference.

- Zonal wind: Quasi-Geostrophic Theory (Pedder, 1997) tells us that in order to determine regions of rising and falling air, we require knowledge of the wind fields at high (e.g. 50hPa) and low pressure levels (e.g. 1000hPa), meaning our choice of levels is physically reasonable.

This agreement with physical reasoning shows that our neural network is able to identify physically important inputs. In addition, the agreement with physical reasoning on level choice shows our neural network can deal with highly correlated time series data. This is because the different pressure levels of a single variable are highly correlated with each other and we are able to identify which pressure levels are important for prediction. Both the agreement with key physical principles and the ability to deal with correlated data are identified in Schultz et al. (2021) as areas where neural networks need to prove themselves in order to be able to compete with numerical weather prediction models. Thus this good agreement with physical reasoning validates our neural network approach.

In summary, in this section we have determined a set of input variables which are important in determining Z500 and T850. From an original dataset of 115 variables, we have been able to exclude 45 through the correlation analysis and a further 36 for Z500 and 37 for T850 through our variable and level importance analysis. Our purely data driven approach agrees with physical reasoning and thus we use this input variable selection in the next section to reduce computational and memory costs without compromising too much on accuracy.

2.3 Neural networks

Previous works have applied several different types of neural networks to this dataset: the original WeatherBench dataset work Rasp et al. (2020) uses a simple convolutional neural network (CNN), Weyn et al. (2020) uses a U-Net (an architecture first described in Ronneberger et al. (2015)), and Rasp and Thuerey (2020) uses a 19-block convolutional ResNet (an architecture first described in He et al. (2016)), which produces the lowest errors of them all. The accuracy improvement given by the convolutional ResNet in Rasp and Thuerey (2020) is to be expected because, as discussed in Lu et al. (2018), a ResNet can be viewed as a variation of the forward Euler finite difference method

$$y_{n+1} = y_n + hf(t_n, y_n), \quad (1)$$

which is actually a much simpler version of the methods used by NWP models to predict the weather (White, 1971). Fundamentally, a neural network provides a way to extract non-linear relationships present in the data and is trained to minimise a loss. This minimisation is done via gradient descent which is used to update the neural network weights. The loss function can play a pivotal role in both neural network's accuracy and efficiency. We have chosen to adopt the latitude-weighted RMSE outlined in Rasp et al. (2020)

$$\text{RMSE} = \frac{1}{N_{\text{hindcasts}}} \sum_{i=1}^{N_{\text{hindcasts}}} \sqrt{\frac{1}{N_{\text{lat}} N_{\text{lon}}} \sum_{j=1}^{N_{\text{lat}}} \sum_{k=1}^{N_{\text{lon}}} L(j) (f_{i,j,k} - t_{i,j,k})^2}, \quad (2)$$

where

$$L(j) = \frac{\cos(\text{lat}(j))}{\frac{1}{N_{\text{lat}}} \sum_{j=0}^{N_{\text{lat}}} \cos(\text{lat}(j))}, \quad (3)$$

is the latitude weighting factor, f is the predicted value from the neural network and t is the true value from the dataset.

Previous works using the WeatherBench dataset have chosen to predict the exact value of the variables Z500 or T850 at a particular point in time, longitude and latitude. An alternative approach is to predict what range they will be in at this time, longitude and latitude. In order to achieve this with a neural network setup, the first step is to convert the continuous weather data to categorical data by taking each target variable and binning its values into 100 bins of equal width. The values of Z500 vary between a minimum of 42 500 m^2s^{-2} and a maximum of 59 300 m^2s^{-2} , meaning that each Z500 bin has width of 169 m^2s^{-2} (to 3 significant figures); T850 varies between 213 K and 314 K, leading to a bin width of 1.02 K (to 3 significant figures). We take the value of the category to be its lowest value, which introduces an inbuilt root mean square error (RMSE) of 91.2 m^2s^{-2} for Z500 data and 0.992 K for T850 data. With the target variables binned, it is then possible to use neural networks used for categorical classification, to predict probability density functions of the variables.

The neural network architecture used in this work is similar to that in Rasp and Thuerey (2020). We use a convolutional ResNet with each residual block consisting of two convolution blocks defined as [2D convolution layer, LeakyReLU layer, Batch normalization layer, Dropout layer]. The LeakyReLU layer is an activation layer with $\alpha = 0.3$ (e.g. Maas et al., 2013) and each Dropout layer uses a dropout rate of 0.1. Following Rasp et al. (2020) and Rasp and Thuerey (2020), the 2D convolutions are defined with periodic padding in the longitude direction and zero padding in the latitude direction but, unlike in those works, each 2D convolution layer has 100 channels (100 bins of categorical

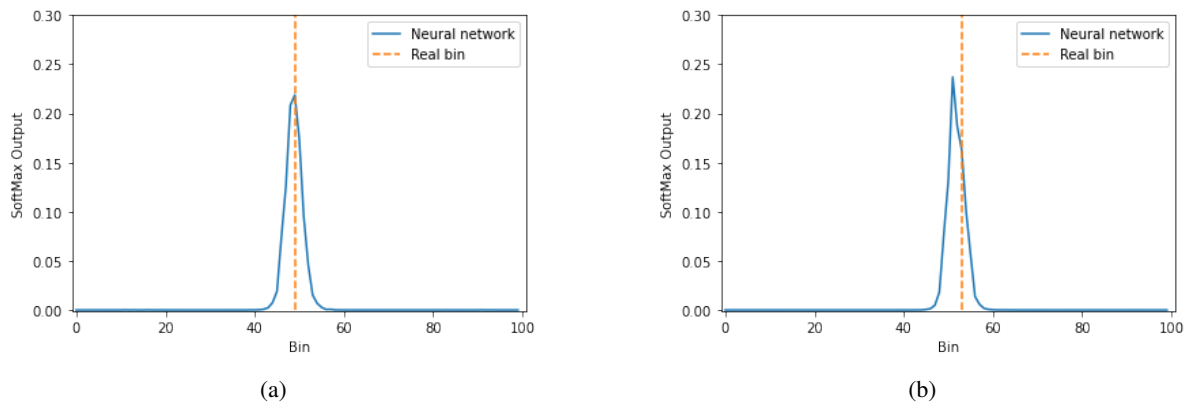


Figure 3: Examples of probability density functions produced by the SoftMax output layer for Z500 data variable (computed with 15 residual blocks).

data) with a kernel size of 5. We use one convolution block at the network input, and we use a SoftMax layer at the output layer, thus obtaining a probability density function for the output variable (Goodfellow et al., 2016). All input data used throughout in the neural network is normalised, but it is not necessary to normalise the output data because it is categorical. Recall that, unless explicitly stated, all results shown in this work refer to the 3-day hindcast.

If we had trained a single neural network to predict both Z500 and T850 at the same time, the SoftMax output layer would mean the output was 5-dimensional. Thus, to avoid memory issues, we train two separate networks to predict them individually, making the output (only) 4-dimensional. Furthermore, we use sparse categorical cross-entropy as the loss metric in keras instead of using one-hot encoding, because the latter would increase the size of an already very large dataset by a factor of 100. The neural network is then compiled using an Adam Optimiser (Kingma and Ba, 2014) with an initial learning rate of $5e-5$, which is reduced by a factor of 0.2 if the validation error does not decrease after 2 epochs. In general, the neural network requires approximately 15 epochs but this varies depending on the set of inputs being trained.

Figure 3 shows how the SoftMax output layer produces a probability density function for a categorical output variable using two random examples. In Figure 3a, the maximum probability bin is the true bin. Although in Figure 3b the maximum probability bin (23.7%) is not the true bin, the true bin has a non-zero probability of 16.3%. This probability density function is a useful tool from a weather-forecasting perspective, because the user knows that the true value has a strong likelihood of occurring.

2.3.1 Comparing categorical data results with continuous data

In order to be able to compare the results of our approach with the correct values from the data and with other neural network and numerical model results, it is necessary to infer a single value from our categorical neural network predictions. To do this, we again take advantage of the probability density function we have predicted and calculate their expectation using

$$\mathbb{E}[X] = \sum_{i=1}^{100} x_i \mathbb{P}(X = x_i), \quad (4)$$

where x_i is chosen to be the lower bound of each bin. In this way, we take advantage of the density functions we have predicted and also reduce the inbuilt error caused by binning the data, which we discussed previously. Throughout this work, the RMSE is calculated between the real data and the expected values of the density functions generated by our approach.

Despite this expectation calculation, there will still be differences caused by using categorical output data compared to continuous data. The simplest way to understand these is by training a series of continuous data and categorical data neural networks with varying numbers of residual blocks and comparing the results. For our initial analysis, we use a training dataset consisting of only the two variables of interest, Z500 and T850 at current time t . Following Rasp and Thuerey (2020), each continuous data neural network has 64 channels in each 2D convolution layer (due to there being 64 longitudes) and a 2D convolution output layer with two channels, meaning that the output has shape (time, 32, 64, 2). In comparison, each categorical data neural network has 100 channels in each 2D convolution layer and a SoftMax output layer, meaning the output has shape (time, 32, 64, 100, 1) (recalling that we train a separate neural network for each output variable for reasons of memory). Note that, for simplicity, initially neither type includes dropout.

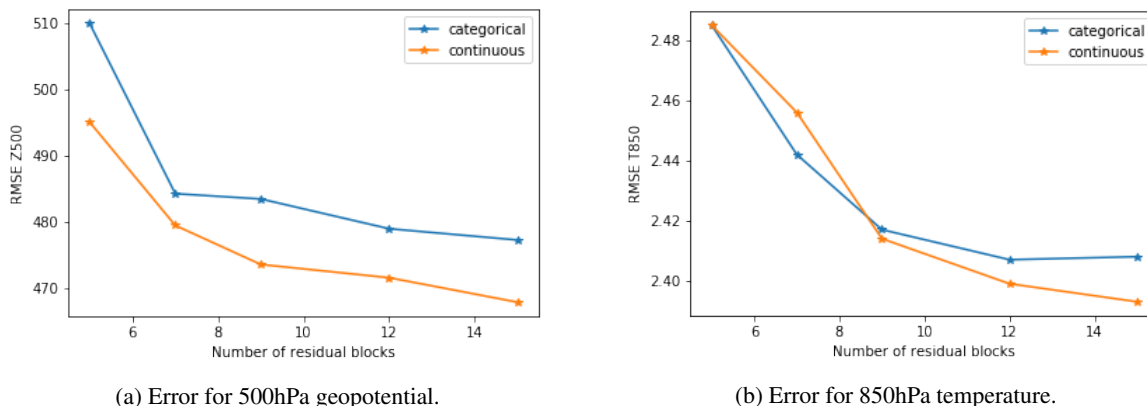


Figure 4: Error from training the neural network with categorical data compared to training with continuous data for different numbers of residual blocks.

Figure 4 shows that the errors decrease as the number of residual blocks increases for both categorical and continuous data. For Z500, Figure 4a shows that the error from training on continuous data is always less than that from training on categorical data, but the difference between the two errors is much less than the inbuilt binning error of $91.2 \text{ m}^2 \text{ s}^{-2}$. For T850, Figure 4b shows that there is little difference in the error as a result of training on categorical data compared to the error from training on continuous data and in fact in one case the categorical data error is lower. This is despite the fact that the inbuilt binning error calculated previously is 0.992 K . This suggests that although working in terms of binned data introduces an error, the new neural network structure and the expectation calculation is able to partially compensate for this.

2.3.2 Using dropout for ensemble modelling

A common strategy to improve the performance of neural networks and, in particular, to prevent overfitting is to use a Dropout layer (e.g. Srivastava et al., 2014). It has the further advantage that if dropout is allowed to occur at the inference phase, an ensemble of outputs can be generated from a single neural network train (Gal and Ghahramani, 2016). This dropout ensemble technique is applied on continuous weather data in Scher and Messori (2020), where they show that using this technique results in an improvement in accuracy. With our approach, because of the SoftMax output layer, each ensemble member is actually a series of density functions at every point in space and time and so careful analysis is required before they are combined. The law of total probability states that

$$\mathbb{P}(A) = \sum_n \mathbb{P}(A|B_i)\mathbb{P}(B_i), \quad (5)$$

if B_i are a finite number of pairwise disjoint sets, whose union is the sample space. In addition, with this technique there is no reason why one ensemble member should be more accurate than the others, and thus a simple average is sufficient to combine them. If we set $\mathbb{P}(A|B_i)$ to be the probability density function from the i th ensemble member and $\mathbb{P}(B_i)$ to be the probability of sampling from the i th distribution (thus $\mathbb{P}(B_i) = 1/n$ where n is total number of ensemble members), we show that averaging the density functions from the ensemble members is mathematically rigorous. This averaging is known as linear pooling (Allard et al., 2012).

Using this knowledge, we can average the ensemble outputs and Figure 5 shows that doing so results in a notable reduction in error when using the dropout ensemble technique compared to not using dropout at all or using dropout but with only one ensemble member. This reduction in error as a result of the dropout ensemble technique is obtained for almost no extra computational cost and occurs no matter the number of residual blocks used. Whilst for T850 the error always decreases as the number of residual blocks increases, for Z500 the error increases when 15 residual blocks are used. This may be due to overfitting and the optimum number of residual blocks will be discussed in more detail in Section 2.3.4. For reference, Figure 5 also shows the error from using the configuration of the Integrated Forecast System (IFS) model of the European Centre for Medium-range Weather Forecasting (ECMWF) at the T42 resolution (approximately 2.8° resolution at the equator) [IFS T42]. This resolution is much coarser than the operational IFS used by ECMWF, but this is a fair comparison because the WeatherBench dataset that we use to train the neural networks also has a coarse resolution (5.625°). Note the IFS T42 value has not been calculated in this work but is taken from Rasp and Thuerey (2020). Thus we have shown that even when using a small training dataset consisting only of Z500 and T850 and 7 residual blocks, the convolutional ResNet with categorical data outputs is substantially more accurate than IFS T42 for both Z500 and T850 when the dropout ensemble technique is used.

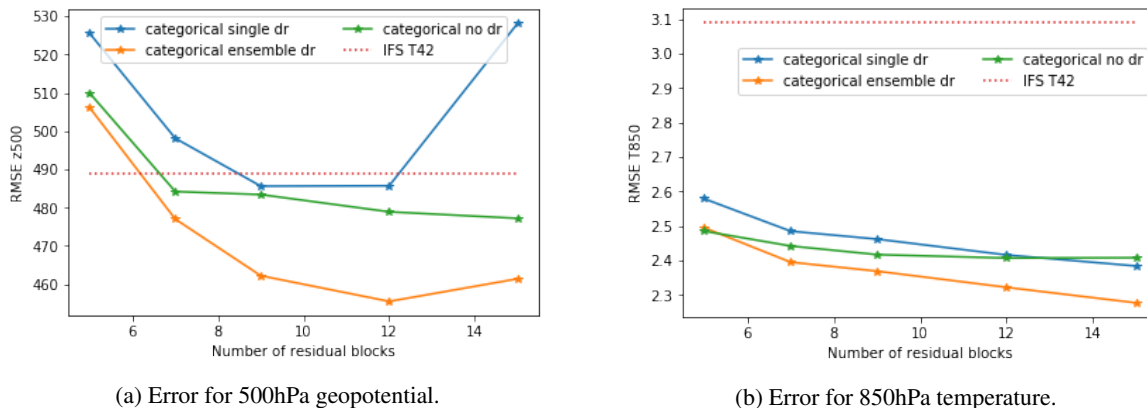


Figure 5: Error as a result of using the dropout ensemble technique; using a single output from a neural network with dropout; using a neural network with no dropout and using the coarse NWP model IFS T42. The ensemble dropout technique outperforms the other techniques for almost all numbers of residual blocks.

2.3.3 Neural Network Stacking

Following Section 2.2, we know which input variables are important to train the neural network. In total, we have identified 34 variables which are important in determining Z500 and 33 important in determining T850 (where for data on multiple levels, we are counting each individual level as a variable). However, memory restrictions mean it is impractical to train a neural network using all the variables that the importance analysis suggested. It should be noted that even if we used all identified variables for our training dataset, it would still be substantially smaller than the 117 variables used in the training dataset in Rasp and Thuerey (2020).

To resolve this issue, instead of training the neural network on all the variables at once, we set-up a series of ResNets (with the same architecture as that described on Section 2.3) on smaller input datasets which always include Z500 and T850 as well as one of (i) optimum geopotential levels; (ii) optimum temperature levels; (iii) optimum potential vorticity levels; (iv) optimum specific humidity levels; (v) optimum zonal wind levels; (vi) constants; (vii) solar radiation (if training for Z500 output), all at current time t . The output of each of these networks is a density function at each point in space and time. To improve accuracy, for each network we use dropout at inference to create an ensemble of 32 outputs and use the law of total probability (5) to average the outputs meaning that the output of each individual neural network run is a single density function output of size (time, 32, 64, 100).

Instead of having separate density function outputs from each input variable combination, we now combine the outputs of these networks to be left with a single output for each point in time and space. There are several different methods to do this including linear pooling with average weights as done with the ensemble created by the dropout. Whilst linear pooling with average weights is sufficient for the dropout ensemble (because there is no reason why one ensemble member should be weighted higher than another), we have seen in Section 2.2 that some input variables are more important than others in determining the final results and thus should have a greater weighting. There are various techniques to combine outputs such as pooling, voting and stacking (Zhou, 2012). We choose to combine our outputs by using the learning technique of stacking (Wolpert, 1992; Smyth and Wolpert, 1999) where a meta-learner (in our case a stacked neural network) is used to combine individual learners (our individual ResNets).

An issue with using this approach to combine our density function outputs is that each density function output is very large – (time, 32, 64, 100) – because each distribution has 100 bins. Thus we may run into memory issues when loading the data for training the stacked neural network. In addition, combining density functions in this way is not guaranteed, and in fact will almost definitely not, output a probability density function because a stacked network does not enforce conditions on the weights to ensure they sum to one, and thus the law of total probability (Eqn. 5) no longer applies. To avoid both of these issues, we transform the density functions from the individual neural networks to expectations using (Eqn. 4). In this way, we still keep the knowledge gained from the density function but reduce the data size to (time, 32, 64, 1). We also avoid any potential issues caused by combining density functions. Figure 6 provides a summary showing how the outputs from individual ResNets are combined using a stacked neural network.

For the stacked neural network, we use a simple shallow network with the following architecture: an input layer to concatenate the output of the individual neural networks, two hidden layers of density 36 with ReLU activation and a SoftMax output layer to generate a probability density function again. As there are now two training stages in our

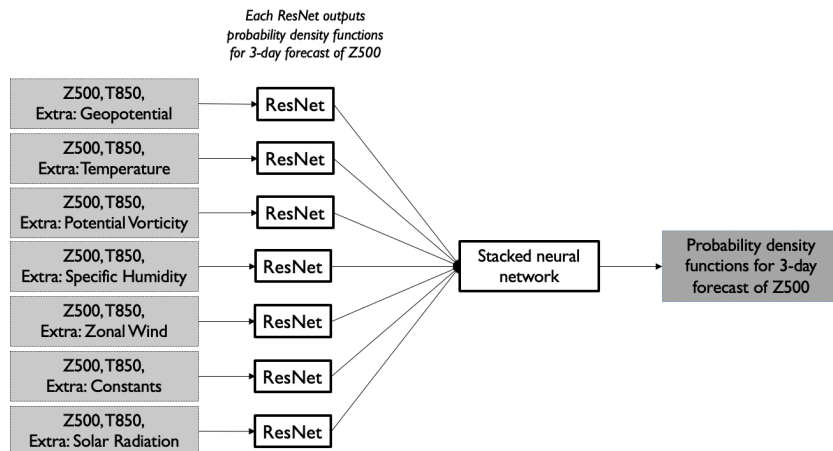


Figure 6: Schematic for Z500 3-day hindcast using the stacked neural network approach to combine outputs from individual ResNets. Note the schematic for the Z500 5-day hindcast, T850 3-day hindcast and T850 5-day hindcast are the same apart from there being no solar radiation Resnet for T850 predictions.

methodology, we require two test datasets. We train each of the individual ResNet learners using the data from 1979 to 2010, and use the data from 2011 as a validation dataset. We then use the individual learners to make predictions on the dataset from 2012 to 2016. These predictions are the inputs for the meta-learner (the stacked neural network), which uses shuffle as validation. As before, the final testing dataset is the data from 2017 to 2018.

2.3.4 Optimum number of residual blocks

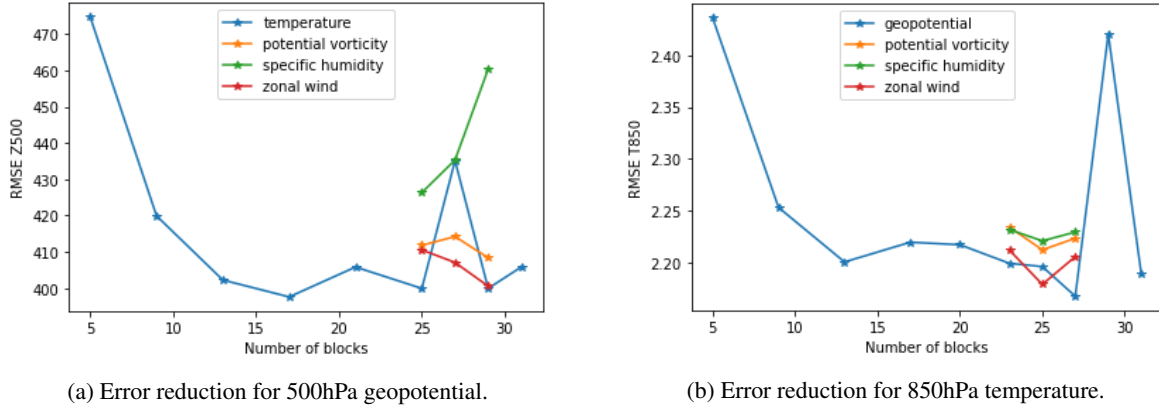
Figures 4 and 5 in the previous sections show that the accuracy of a ResNet is very dependent on the number of residual blocks used. Thus, the final factor that we need to determine before applying our methodology to the WeatherBench data is the optimum number of residual blocks to use in the individual ResNets which feed the stacked neural network.

Figure 7a and 7b show how RMSE Z500 and RMSE T850 vary as the number of residual blocks is increased. The error is calculated on the 2012 to 2016 dataset, because these are the predictions which are used as the input for the stacked neural network. For the main analysis of the optimum number of blocks, we use the optimum temperature levels as the training dataset for Z500 and the optimum geopotential levels as the training dataset for T850. Before 25 residual blocks, in both cases the error decreases relatively steadily as the number of residual blocks increases. However, beyond this number the error sometimes increases dramatically when more residual blocks are added and sometimes decreases dramatically. Thus we also conduct a small sensitivity analysis using the optimum levels of potential vorticity, specific humidity and zonal wind, the results of which are also shown on Figures 7a and 7b. This confirms that for Z500, the optimum number of residual blocks is 29 and for T850, the optimum number of residual blocks is 25.

3 Results

In the previous section, we outlined our new methodology for predicting the weather forecast using a purely data-driven approach. In this section, we show the results of implementing this methodology. As discussed previously, all the analysis so far has been carried out for the 3-day weather hindcast but we show that this methodology also leads to good results for the 5-day weather hindcast.

Figures 8a and 8b compare, for Z500 and T850 respectively, the 3-day prediction error on the test dataset from using each of the individual learners trained on a specific variable, simply averaging the output from the individual ResNets and using the stacked neural network to combine the outputs. Figures 9a and 9b show the same comparison for the 5-day prediction error on the test dataset. These figures show that for both the 3-day and 5-day hindcast for both Z500 and T850, the stacked neural network always provides the most accurate result and the error is notably reduced through using it. Unlike when we simply average the outputs, the stacked neural network is not adversely influenced by the presence of individual ResNets with much larger errors than others, (for example in Figure 8a where the error when using solar radiation is much larger). This is because it learns in training to give a lower weight to these outputs and

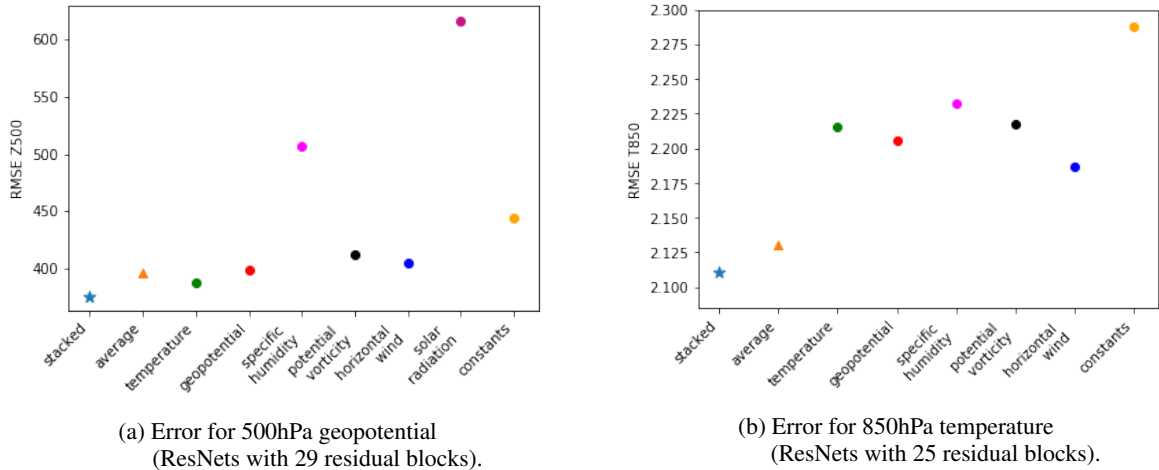


(a) Error reduction for 500hPa geopotential.

(b) Error reduction for 850hPa temperature.

Figure 7: Determining the optimum number of residual blocks to use in the ResNet.

thus the overall error is unaffected. In addition, the stacked neural network is computationally cheap to train because of its simple architecture and thus we achieve these accuracy improvements for very little extra computational cost.



(a) Error for 500hPa geopotential (ResNets with 29 residual blocks).

(b) Error for 850hPa temperature (ResNets with 25 residual blocks).

Figure 8: Improvement in accuracy for the 3-day hindcast as a result of using a stacked neural network compared to the individual ResNets trained on specific variables and simply averaging the outputs.

To visualise what these error values mean, we look at the specific event of Storm Ophelia which was an active storm between 9th-18th October 2017, and the worst storm to affect Ireland in over 50 years (Stewart, 2017). Figure 10 focuses on the North Atlantic region and compares the true value from the data with the 3-day and 5-day hindcasts for Z500 and T850 at 00UTC 17 October 2017, which was when the storm was affecting the British Isles. It is clear that for both the 3-day and 5-day hindcast, the neural network can predict the general distribution of Z500 and T850 well. Unsurprisingly, the 3-day hindcast is more accurate and is able to pick up finer details not present in the 5-day hindcast.

Finally, in Table II, we summarise the results from using our stacked neural network and compare them with results from using simple methods (persistence and weekly climatology), other neural networks (Weyn et al., 2020; Rasp and Thuerey, 2020) and numerical models (IFS T42 and operational IFS) where the numerical model results have been taken from Rasp et al. (2020). The key finding shown in this table is that our approach is approximately as accurate as that in Weyn et al. (2020) despite the fact that our neural network has a simpler setup than the U-Net approach used in Weyn et al. (2020) and we are using categorical data rather than continuous data which adds an inbuilt error to our results. This highlights the advantages we gain from the data exploration and good choice of neural network architecture described in Section 2. The table also shows that our approach is more accurate than the numerical IFS T42 model and the simple methods of persistence and weekly climatology, but less accurate than the neural network approach in Rasp and Thuerey (2020) and the operational IFS model. It is likely that our neural network's lower skill compared to Rasp and Thuerey (2020) is due to the fact that Rasp and Thuerey (2020) model

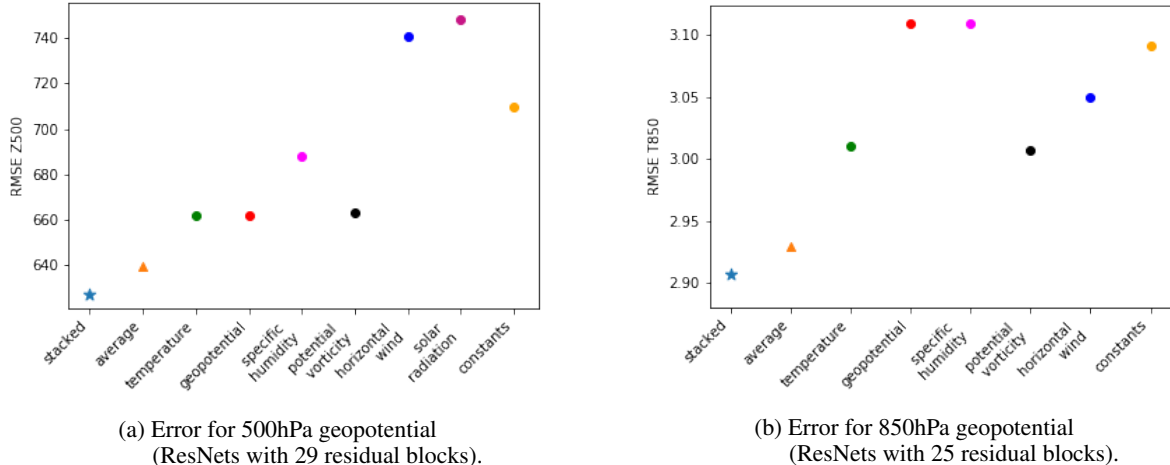


Figure 9: Improvement in accuracy for the 5-day hindcast as a result of using a stacked neural network compared to the individual ResNets trained on specific variables and simply averaging the outputs.

is trained on a much larger dataset of the WeatherBench data (117 data variables compared to our training dataset of 34 data variables for Z500 and 33 data variables for T850) and is also pretrained on extra data from the Climate Model Inter-comparison Project (CMIP) (see Eyring et al., 2016). Thus the approach in Rasp and Thuerey (2020) is both much more computationally expensive and much more memory intensive than our approach. Furthermore, our approach has introduced improvements which combine dropout based ensembles with the ability to predict probability density functions instead of single values. In the next section, we show how this enables us to make a more informed weather forecast.

	RMSE Z500 (3-day/5-day)	RMSE T850 (3-day/5-day)
Stacked neural network	375/627	2.11/2.91
Persistence	936 / 1033	4.23 / 4.56
Weekly Climatology	816	3.5
IFS T42	489 / 743	3.09 / 3.83
Weyn et al. (2020)	373 / 611	1.98 / 2.87
Rasp and Thuerey (2020)	268 / 499	1.65 / 2.41
Operational IFS	154 / 334	1.36 / 2.03

Table II: Error for 3-day and 5-day hindcasts for Z500 and T850 comparing the results from using our approach in bold, with simple methods (persistence and weekly climatology), numerical models (IFS T42) and other neural networks (Weyn et al., 2020; Rasp and Thuerey, 2020).

3.1 Estimating uncertainty

A common criticism of using neural networks for weather forecasting is that they are unable to estimate the uncertainty of the forecast (Schultz et al., 2021). Thus, one of the key novelties of our neural network approach to predicting the weather is that unlike in previous works, we produce a probabilistic output, through our prediction of a probability density function for the variable of interest. This probabilistic output enables us to estimate uncertainty and obtain notably more information from our neural network predictions.

To visualise the probabilistic output, we again consider the example of Storm Ophelia. Figures 11a and 11c show the cumulative distribution function (CDF) for T850 from 3 and 5-day hindcasts at 00UTC 17 Oct 2017. In each panel, the CDFs for three different thresholds are shown using probability contours. These probability contours indicate the locations where the probability of T850 being lower than 263.15 K (-10°C) (red), 273.15 K (0°C) (green) and 283.15 K (10°C) (blue) is 0.1, 0.5 and 0.9. Similarly Figures 11b and 11d show equivalent probability information for Z500. Note that, although for a given threshold the probability contours will never cross, the probability contours of different thresholds may cross.

In effect, Figures 11a and 11c shows the median location of the 3 isotherms as well as the 10 to 90% probability interval. We see meanders in the contours associated with mid-latitude synoptic systems, and locations where the

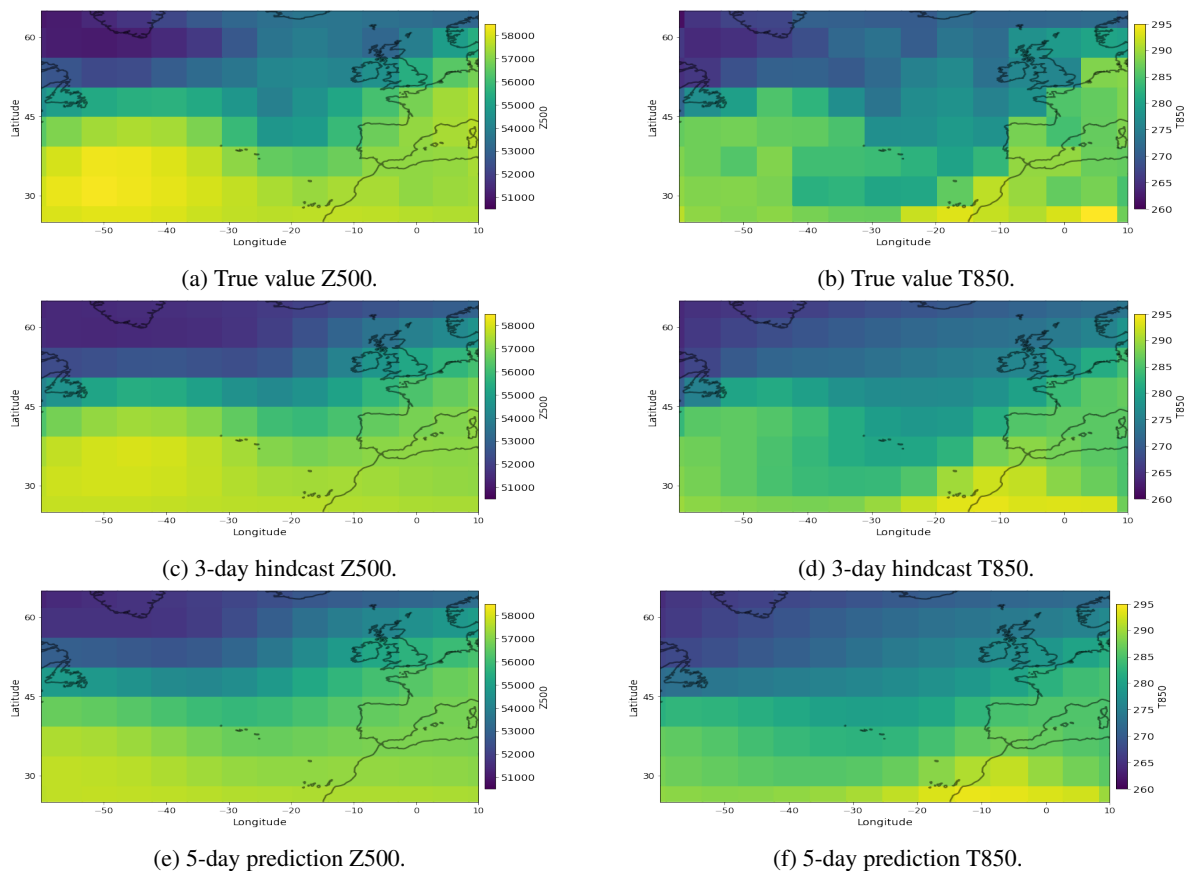


Figure 10: Comparing true Z500 and T850 with 3-day and 5-day hindcast at 00UTC 17 October 2017 during Storm Ophelia.

probabilities are not symmetric about the median (e.g. in the 3-day T850 hindcast off the west coast of California, where the distance between the 90% and 50% contours is larger than between the 50% and 10% contours for the probability of T850 being less than 283.15 K (10°C)). The CDF for the thresholds of 263.15, 273.15, 283.15 K chosen here, generally do not overlap in the 3-day T850 hindcasts in Figure 11a. However, in the 5-day T850 hindcasts, where there is more uncertainty, the spread in each set of contours is wider and there are places where they do overlap (e.g. over Iceland, where there is a 90% chance of T850 being lower than 273.15 K (0°C) but also a 10% chance that it is lower than 263.15 K (-10°C)). For Z500, in Figures 11b and 11d, we also see the contours are closer together in the 3-day hindcast compared to the 5-day hindcast, indicating more certainty in the 3-day prediction.

The probabilistic output of the neural network also means we can estimate uncertainty and skill metrics (Hudson and Ebert, 2017) for our predictions. For example, we can calculate the Brier score (Brier, 1950) given by

$$\text{Brier score} = \frac{1}{N} \sum_{i=1}^N (p_i - o_{i_{\text{true}}})^2, \quad (6)$$

where N is the number of bins, p_i is the probability that the bin is correctly predicted by the neural network and $o_{i_{\text{true}}}$ is the true probability and thus is equal to 0 apart from for the correct bin where it is 1. The minimum Brier score possible is 0 and the maximum 1 – the closer the value is to 0 the better the predictions are calibrated. For our predictions, each datapoint in space and time has its own density function and hence its own Brier score and in Figure 12, we show the density function of these scores for the Z500 and T850, 3-day and 5-day hindcasts. In all cases, we see the Brier score is very close to 0 indicating the predictions are well calibrated. For both Z500 and T850, the 3-day hindcast scores are generally smaller than the 5-day hindcast indicating, unsurprisingly, that the 3-day hindcast is generally better calibrated.

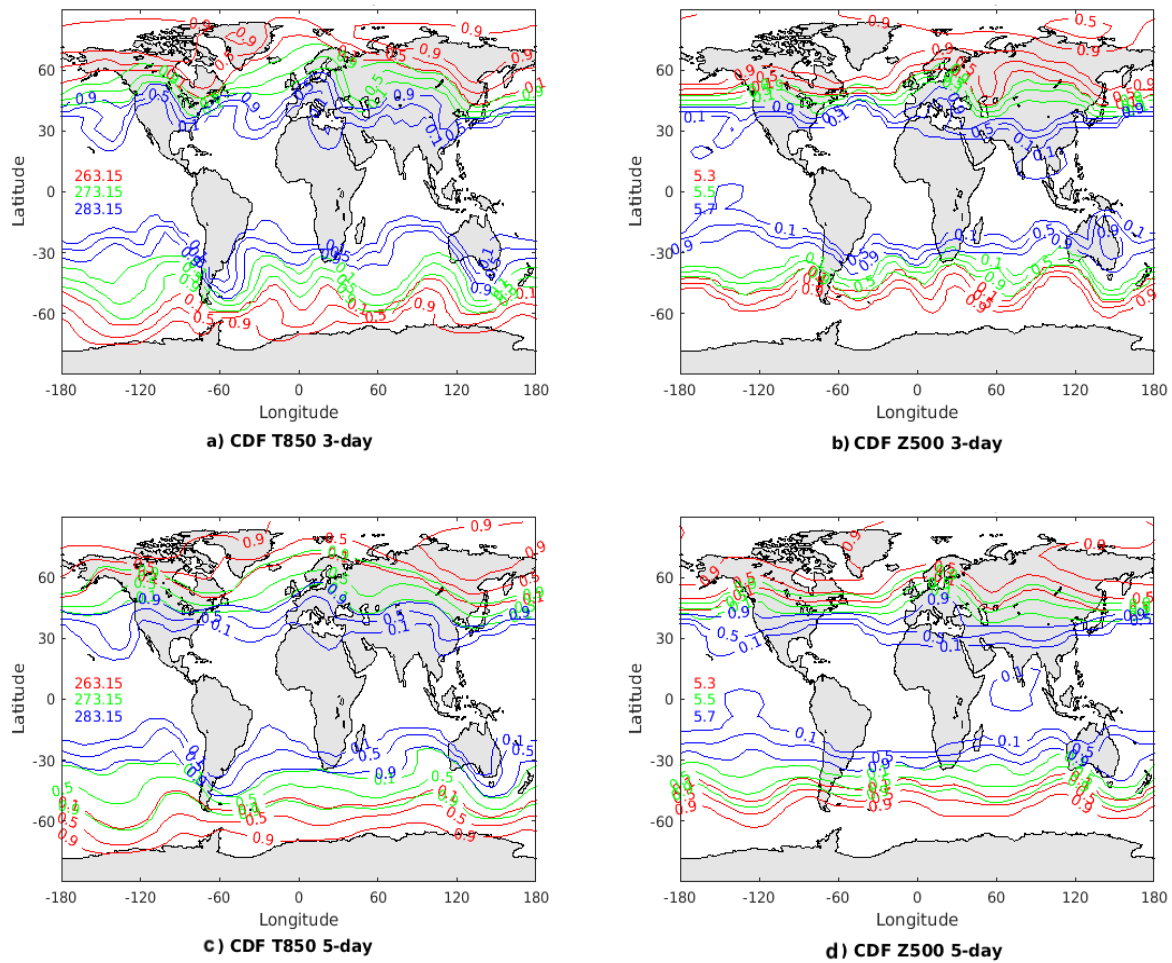


Figure 11: Contour maps of the cumulative distribution functions at 00UTC 17 Oct 2017. Contours are at 0.1, 0.5 and 0.9. For T850 the thresholds considered are T850 ; 263.15 K (red), T850 ; 273.15 K (green) and T850 ; 283.15 K (blue) and for Z500 they are Z500 ; $5.3 \times 10^4 m$ (red), Z500 ; $5.5 \times 10^4 m$ (green) and Z500 ; $5.7 \times 10^4 m$ (blue).

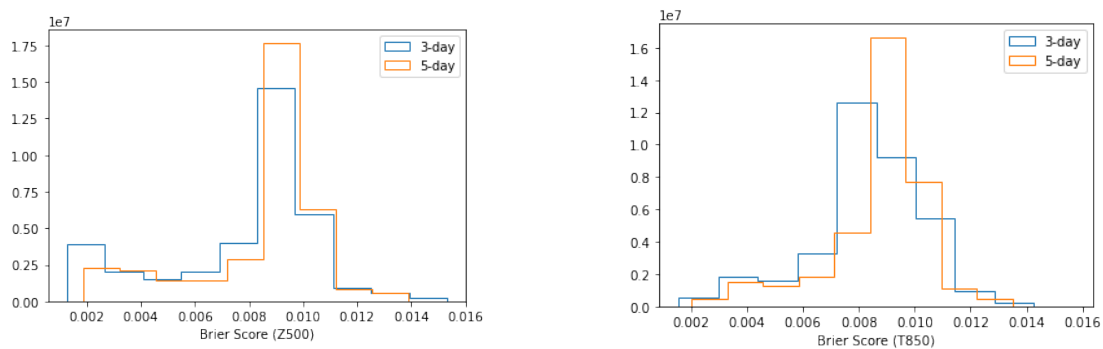


Figure 12: Brier Scores for the probability density functions predicted by our neural network methodology Left: Z500; Right: T850. Note the smaller the value the better calibrated the predictions.

	Z500 (3-day)	T850 (3-day)	Z500 (5-day)	T850 (5-day)
Within 95% confidence interval	13.8%	17.2%	14.7%	17.3%
Within 99% confidence interval	16.3%	20.3%	17.4%	20.5%
Within one σ	64.7%	71.2%	67.3%	71.2%
Within two σ	93.6%	94.0%	94.0%	94.2%

Table III: Percentage of datapoints where the true value is within a set interval from the expected value predicted by the neural network.

Another metric we can calculate is the standard deviation, σ , of our density functions. We do this using

$$\sigma = \sqrt{\sum_{i=1}^{100} (x_i - \mu)^2 \mathbb{P}(X = x_i)}, \quad (7)$$

where μ is the expectation of X given by (Eqn. 4) and, as before, the value of each bin x_i is taken to be the lower bound. This informs on the spread of the distribution and allows us to calculate the confidence intervals using

$$\mu \pm Z \frac{\sigma}{\sqrt{N}}, \quad (8)$$

where N is the number of bins and Z is the z -value taken from the normal distribution and equal to 1.960 for the 95% confidence interval and 2.576 for the 99% confidence interval. In Table III, we show the percentage of datapoints in time and space where the true value is within the 95% confidence interval and 99% confidence interval around the predicted expected value. The proportions are relatively low but it should be noted that the standard deviation of the density function is on average very small because as shown in Figure 3, the distributions are very centred around the expected value – the average width for the 99% confidence interval is 0.6 K and 0.8 K for the T850 3-day and 5-day hindcast respectively (smaller than the width of one bin) and 100 hPa and 160 hPa for the Z500 3-day and 5-day hindcast respectively (approximately the same size as the width of one bin). Therefore, we also show in Table III, the proportion of true values within one and two σ of the predicted expected value. The majority of true values are within one σ of the expected value and almost all (over 90%) are within two σ . These metrics, and others like it, help practitioners determine how much confidence to have in the predictions and also allow them to understand the confidence they should have in neural network results compared to other model results.

Finally, the probability density functions not only improve understanding of the spread and skill of the results but also inform of scenarios which are not the most likely to occur, but still have a relatively high probability of doing so. Recall from the example in Figure 3b, that in that case the bin the neural network predicts with the highest probability is not the correct bin, but the correct bin still has a high probability of occurring. Figure 13 quantifies cases like these. The first bar in all four subfigures shows the percentage of datapoints for which the bin with the predicted highest probability is the correct bin – in all four cases this is over 20%. The second bar shows the percentage of datapoints where the correct bin is either the bin with the predicted highest probability or the predicted second highest probability of occurring. This continues until the fifth bar of the subfigures which shows the percentage of datapoints where the correct bin is one of the top 5 bins that the neural network predicts is most likely to occur. For the 3-day predictions, the correct bin is in one of the top 5 most likely to occur for almost 80% of the datapoints and for the 5-day predictions, the correct bin is one of the top 5 most likely for over 60% of the datapoints. Given that there are 100 bins such a high proportion from just the top 5 is a notable result. It means that in the vast majority of cases, the true scenarios have a high probability associated with them, which enables practitioners to make informed decisions when forecasting and issuing weather warnings.

Thus we have shown in this section how much more information can be gained for weather forecasting if the neural network predicts density functions rather than single values.

4 Conclusion

In this work, we have shown for the first time how neural networks can be used to predict probability density functions instead of single values for weather output variables. This enables practitioners to estimate the uncertainty of the neural network predictions and to provide a more informed weather forecast. In particular, the probability density functions inform about events which, although may not be the most likely to occur, still have a high probability of happening. We have thus provided a solution to a major concern that many practitioners have regarding the use of neural networks for weather forecasting (see Schultz et al., 2021).

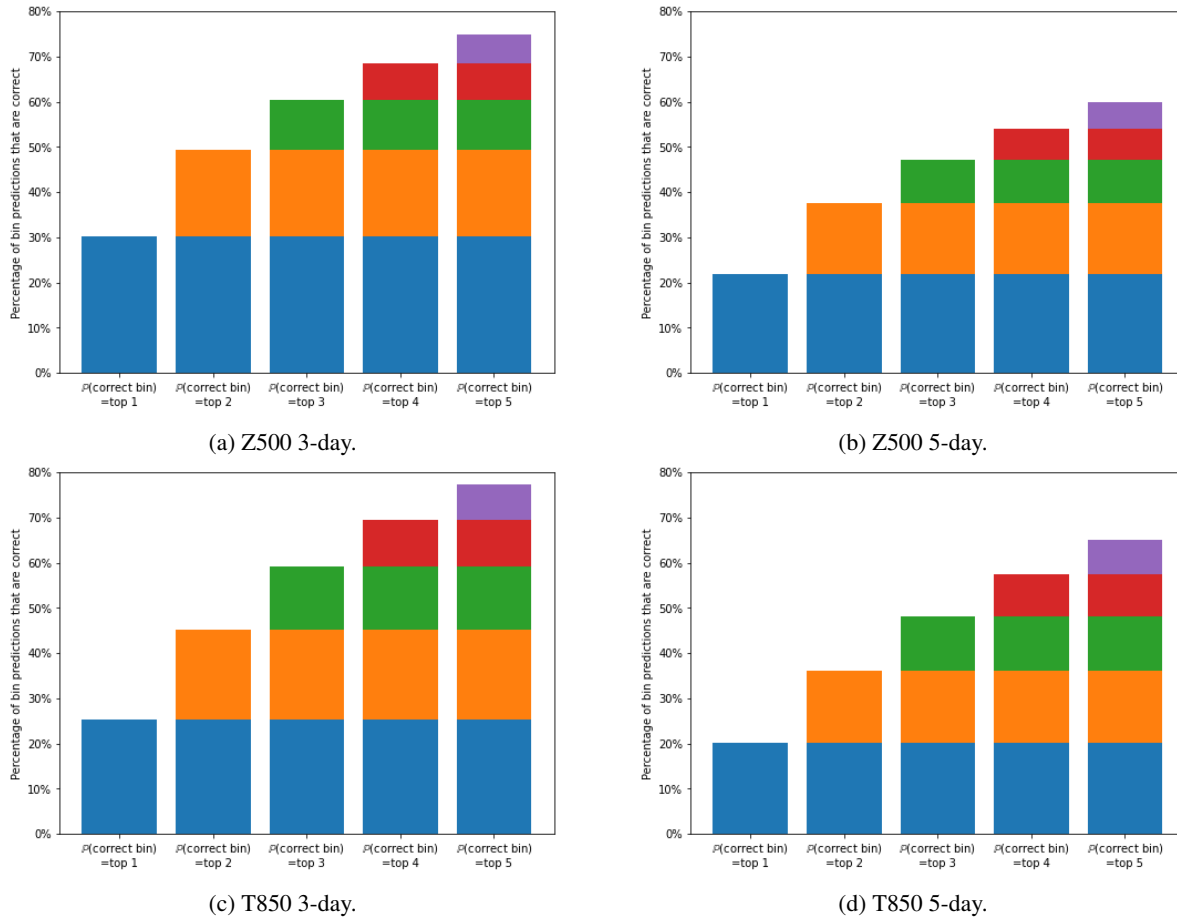


Figure 13: Percentage of all datapoints in time and space where the probability predicted by the neural network for the correct bin is one of the top 1-5 probabilities out of 100.

For our neural network predictions, a relatively simple ResNet has been used and carefully optimised to improve the accuracy of our results. Through the careful choice of this architecture along with extensive data exploration, we have shown that our predictions are more accurate than some coarse NWP models, and as accurate as those in Weyn et al. (2020) which uses a more complex neural network architecture. We have also shown that the important variables identified by the data exploration agree with physical reasoning, thereby validating our neural network approach. It also shows that, even though it is purely data-driven, the neural network is capable of learning physical principles. Moreover, our novel use of a stacked neural network to combine outputs for weather forecasting reduces memory cost, as well as computational cost, and means that less powerful computers are required to make predictions.

Finally, in this work we have shown that transforming our output data to categorical can still give accurate results for continuous numerical weather data. We have shown that it is possible to move beyond point estimates for neural networks based weather forecasts and produce a probabilistic forecast by combining multiple smaller more efficient models. This opens up a new avenue of research for purely data-driven weather forecasting, where ever bigger models trained with enormous datasets is not the only way to achieve model skill. In future work, we will seek to explore the use of transfer learning to further improve the training efficiency of the neural networks.

Computer Code availability

The relevant code for the neural networks presented in this work can be found at https://github.com/mc4117/ResNet_Weather.git.

References

- Allard, D., Comunian, A., and Renard, P. (2012). Probability aggregation methods in geoscience. Mathematical Geosciences, 44(5):545–581.
- Bauer, P., Thorpe, A., and Brunet, G. (2015). The quiet revolution of numerical weather prediction. Nature, 525(7567):47–55.
- Bihlo, A. (2021). A generative adversarial network approach to (ensemble) weather prediction. Neural Networks.
- Brenowitz, N. D. and Bretherton, C. S. (2019). Spatially Extended Tests of a Neural Network Parametrization Trained by Coarse-Graining. Journal of Advances in Modeling Earth Systems, 11(8):2728–2744.
- Brier, G. W. (1950). Verification of forecasts expressed in terms of probability. Monthly weather review, 78(1):1–3.
- Buda, A. (2011). Life time of correlation between stocks prices on established and emerging markets. arXiv preprint arXiv:1105.6272.
- Dueben, P. D. and Bauer, P. (2018). Challenges and design choices for global weather and climate models based on machine learning. Geoscientific Model Development, 11(10):3999–4009.
- Eyring, V., Bony, S., Meehl, G. A., Senior, C. A., Stevens, B., Stouffer, R. J., and Taylor, K. E. (2016). Overview of the coupled model intercomparison project phase 6 (cmip6) experimental design and organization. Geoscientific Model Development, 9(5):1937–1958.
- Gal, Y. and Ghahramani, Z. (2016). Dropout as a Bayesian Approximation: Representing Model Uncertainty in Deep Learning. In 33rd International Conference on Machine Learning, pages 1050–1059, New York, USA.
- Goodfellow, I., Bengio, Y., Courville, A., and Bengio, Y. (2016). Deep learning. MIT press Cambridge.
- He, K., Zhang, X., Ren, S., and Sun, J. (2016). Deep residual learning for image recognition. In Proceedings of the IEEE conference on computer vision and pattern recognition, pages 770–778.
- Hersbach, H., Bell, B., Berrisford, P., Hirahara, S., Horányi, A., Muñoz-Sabater, J., Nicolas, J., Peubey, C., Radu, R., Schepers, D., et al. (2020). The era5 global reanalysis. Quarterly Journal of the Royal Meteorological Society, 146(730):1999–2049.
- Hoskins, B. (2015). Potential vorticity and the pv perspective. Advances in Atmospheric Sciences, 32(1):2–9.
- Hoskins, B., Draghici, I., and Davies, H. (1978). A new look at the ω -equation. Quarterly Journal of the Royal Meteorological Society, 104(439):31–38.
- Hudson, D. and Ebert, B. (2017). Ensemble verification metrics. In Proceedings of the ECMWF Annual Seminar, Reading, UK, pages 11–14.
- Kingma, D. P. and Ba, J. (2014). Adam: A method for stochastic optimization. arXiv preprint arXiv:1412.6980.
- Konecny, P. and Pustka, D. (2017). Random variation and correlation of the weather data series-evaluation and simulation using bounded histograms. In MATEC Web of Conferences, page 00085. EDP Sciences.
- Lu, Y., Zhong, A., Li, Q., and Dong, B. (2018). Beyond finite layer neural networks: Bridging deep architectures and numerical differential equations. In International Conference on Machine Learning, pages 3276–3285. PMLR.
- Maas, A. L., Hannun, A. Y., and Ng, A. Y. (2013). Rectifier nonlinearities improve neural network acoustic models. In Proc. icml, volume 30.
- Pedder, M. A. (1997). The omega equation: Q-g interpretations of simple circulation features. Meteorological Applications: A journal of forecasting, practical applications, training techniques and modelling, 4(4):335–344.
- Rasp, S., Dueben, P. D., Scher, S., Weyn, J. A., Mouatadid, S., and Thuerey, N. (2020). Weatherbench: A benchmark data set for data-driven weather forecasting. Journal of Advances in Modeling Earth Systems, 12(11):e2020MS002203.
- Rasp, S. and Thuerey, N. (2020). Purely data-driven medium-range weather forecasting achieves comparable skill to physical models at similar resolution.
- Ronneberger, O., Fischer, P., and Brox, T. (2015). U-net: Convolutional networks for biomedical image segmentation. In International Conference on Medical image computing and computer-assisted intervention, pages 234–241. Springer.
- Scher, S. and Messori, G. (2018). Predicting weather forecast uncertainty with machine learning. Quarterly Journal of the Royal Meteorological Society, 144(717):2830–2841.
- Scher, S. and Messori, G. (2020). Ensemble methods for neural network-based weather forecasts. Journal of Advances in Modeling Earth Systems, pages 1–17.

- Schultz, M. G., Betancourt, C., Gong, B., Kleinert, F., Langguth, M., Leufen, L. H., Mozaffari, A., and Stadtler, S. (2021). Can deep learning beat numerical weather prediction? Philosophical Transactions of the Royal Society A: Mathematical, Physical and Engineering Sciences, 379:20200097.
- Smyth, P. and Wolpert, D. (1999). Linearly combining density estimators via stacking. Machine Learning, 36(1):59–83.
- Srivastava, N., Hinton, G., Krizhevsky, A., Sutskever, I., and Salakhutdinov, R. (2014). Dropout: a simple way to prevent neural networks from overfitting. Journal of machine learning research, 15(1):1929–1958.
- Stewart, S. R. (2017). Hurricane Ophelia - tropical cyclone report. Technical report, National Hurricane Center.
- Wallace, J. and Hobbs, P. (1977). Atmospheric science: An introductory survey academic press. New York, 467.
- Wang, X. and Wang, K. (2014). Estimation of atmospheric mixing layer height from radiosonde data. Atmospheric Measurement Techniques, 7(6):1701–1709.
- Weyn, J. A., Durran, D. R., and Caruana, R. (2020). Improving data-driven global weather prediction using deep convolutional neural networks on a cubed sphere. Journal of Advances in Modeling Earth Systems, 12(9):e2020MS002109.
- White, P. W. (1971). Finite-difference methods in numerical weather prediction. Proceedings of the Royal Society of London. Series A, Mathematical and Physical Sciences, 323(1553):285–292.
- Wolpert, D. H. (1992). Stacked generalization. Neural networks, 5(2):241–259.
- Yassaghi, H., Mostafavi, N., and Hoque, S. (2019). Evaluation of current and future hourly weather data intended for building designs: A Philadelphia case study. Energy and Buildings, 199:491–511.
- Yuval, J. and O’Gorman, P. A. (2020). Stable machine-learning parameterization of subgrid processes for climate modeling at a range of resolutions. Nature Communications, 11(1):1–10.
- Zhou, Z.-H. (2012). Ensemble methods: foundations and algorithms. CRC Press, Taylor & Francis Group, Boca Raton, Florida, USA.